PERFORMANCE OF A RAW HEMATITE AND A MANUFACTURED COPPER-IRON OXYGEN CARRIER IN A 50-KW NATURAL GAS CHEMICAL LOOPING SYSTEM

Samuel Bayham, Justin Weber, Doug Straub, Ronald Breault*

National Energy Technology Laboratory, 3610 Collins Ferry Rd, Morgantown, WV, USA 26507-0880

*Email: *ronald.breault@netl.doe.gov*

Abstract – In this work, performance results are presented from the operation of a 50-kW_{th} natural gas chemical looping facility using a raw hematite ore and a manufactured copper-iron-alumina carrier. The parameters measured include the flue gas compositions and molar flow rates, fuel conversion, and oxygen carrier conversion (amount of oxygen utilized). These parameters are compared between the two carriers, and changes in parameters such as reactor temperature, residence times, etc. on the fuel conversions are discussed. The methane conversion for the hematite ore ranged between 9-35%, depending on the gas residence time, temperature, and natural gas feed fraction. The operation of the manufactured copper-iron-alumina carrier required a lower operating temperature than the hematite because of the presence of copper, namely between 751-844°C. For the copper-iron material, the methane conversion to CO_2 ranged from 33.9% to 76.5%, which is significantly higher than the hematite, despite the lower operating temperature range. Additionally, the solids circulation rate for the manufactured copper-iron carrier was several times lower than circulation rate for the raw hematite carrier.

INTRODUCTION

Chemical looping combustion has been proposed as an efficient and cost-effective carbon capture technology and as an alternative to oxy-combustion. The technology splits the oxidation of carbonaceous fuels into two steps by reducing and oxidizing a solid metal oxide, preventing the direct mixing of air with the fuel and thereby eliminating the energy penalty required for separating the carbon dioxide from the molecular nitrogen, as shown in Fig. 1. The technology is being pursued at the National Energy Technology Laboratory (NETL) as a potentially transformational technology (Ciferno et al., 2011). The major challenges for developing the technology are finding a reactive yet mechanically durable oxygen carrier and designing a practical system that allows for controlled solids circulation between the air and fuel reactors and provides gas sealing between the two reactors.

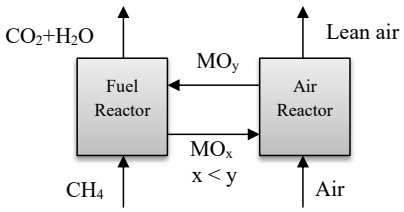

Fig. 1. Chemical looping combustion with natural gas as the fuel.

The literature describes various groups developing and studying oxygen carriers for chemical looping combustion. According to Adanez et al. (2012), it is estimated that there have been over 700 carriers formulated prior to 2010. Many of these carriers are tested and developed at small scale in a laboratory. While these materials may have high reactivity at small scale, performance at larger scale may not be ideal, both in terms of reactivity and mechanical integrity. Thus, many researchers have developed circulating test units to evaluate the novel oxygen carriers under conditions more representative of a scaled-up process, such as those described by Linderholm et al. (2016), Adanez (2006), and Shen (2009). NETL has also designed and constructed a small integrated test facility with a natural gas thermal input of approximately 50 kW_{th}. In this work, two representative oxygen carriers are tested: 1) a raw hematite ore, and 2) a synthetic copper-iron-alumina oxygen carrier designed for high fuel conversion and durability.

EXPERIMENTAL SETUP

NETL has constructed a 50-kW_{th} natural gas fed Chemical Looping Reactor to test potential oxygen carriers under conditions more representative of a scaled-up system (Weber et al., 2014). A sketch of the 50 kW_{th} chemical looping system is shown in Fig. 2, along with a picture for reference. The unit consists of an 8-inch bubbling fluidized bed fuel reactor and a 6-inch fluidized bed air reactor, which can be operated either in bubbling or turbulent regime, and the reactors are sealed by a small fluidized bed below the air cyclone called the seal pot, which is 8-inch in diameter. The system is refractory-lined in a carbon steel shell.

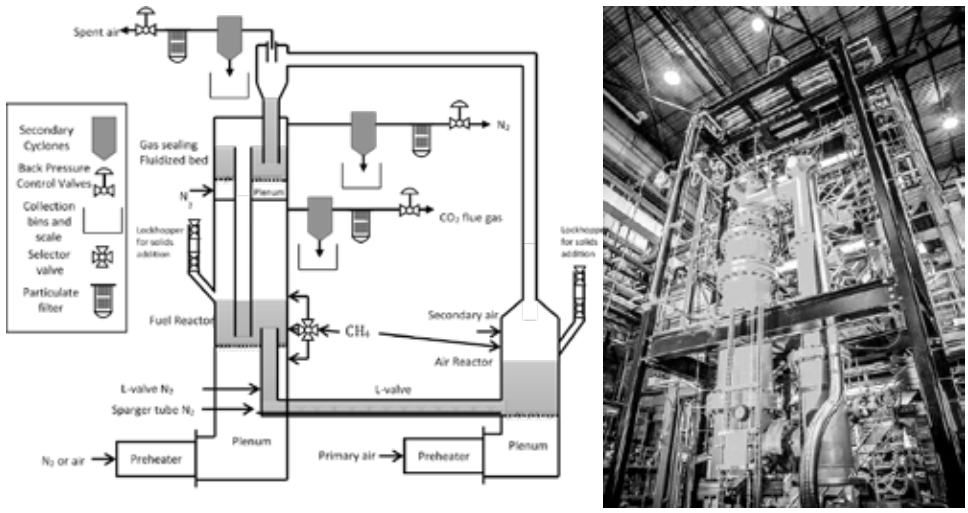

Fig. 2. Chemical looping reactor at NETL

Solids react in the fuel reactor with the natural gas diluted with nitrogen. The solids exit the fuel reactor near the bottom through an L-valve aerated with nitrogen. A sparger in the horizontal section of the L-valve helps propagate the solids across the L-valve. The solids exit the L-valve near the bottom of the air reactor, where they are fluidized by air. In the air reactor, preheated air is used to fluidize the particles and control the heat of combustion reaction, while secondary air is added near the top of the bed to entrain the solids into a riser. The solids pass through the riser and into a cyclone. The dipleg of the cyclone extends into the seal pot. The fluidized solids exit the seal pot through an overflow standpipe and enter the fuel reactor to complete the chemical looping cycle. Except for the preheated air and the heat of reaction, no external heat is supplied directly to the solids flow path.

The three gas outlets (fuel reactor, cyclone, seal pot) each contain secondary cyclones that collect entrained solids, followed by a particulate filter. The solids collected from the secondary cyclones are weighed when they leave the system. Back-pressure control valves are installed for each of the three outlets. The pressure in the air reactor is controlled based on the global (static) pressure, while the pressures in the fuel reactor and seal pot are controlled based on differential pressure to ensure that the pressure in the seal pot is slightly higher than the cyclone. All the gas inlets are preheated to around 600°C and controlled using mass flow controllers (Alicat Scientific). Natural gas can be added to both the air and fuel reactors.

Startup of the system consists of heating the refractory with air heated by the electric preheaters at a slow rate (50°C/hr) with no solids in the vessel. Once the temperature exceeds the autoignition temperature of natural gas, then natural gas is slowly added to the empty vessel to heat the system to the desired operating temperature. Once the desired temperature is reached, solids are slowly added through the lockhoppers until the desired inventory is reached. Solids circulation is initiated by fluidizing all three reactors and adding aeration gas to the L-valve. When the desired circulation rate is attained, chemical looping trials commence by replacing the air in the fuel reactor with nitrogen.

Gases are sampled from the gas outlets of all three fluidized vessels. In the exhaust of the fuel reactor, CH_4, CO_2, and CO are measured continuously using non-dispersive infrared analyzers. O_2 is also measured using a paramagnetic analyzer. A gas chromatograph also measures N_2 and H_2 exiting the fuel reactor every 90 seconds. In the air reactor exhaust, CO_2 and O_2 are continuously measured, and CO_2 is measured in the seal pot exhaust.

For the fuel reactor, the molar flow rates of the individual gas species are calculated assuming a closed nitrogen and hydrogen balance. The total outlet flowrate on a dry basis is calculated by dividing the total flowrate of nitrogen at the inlet by the volume fraction of nitrogen in the flue gas:

$$Q^*_{\mathrm{T,dry}} = \frac{Q^*_{\mathrm{N_2,in}}}{y_{\mathrm{N_2,out,dry}}} \tag{1}$$

The molar flowrate of each species in the fuel reactor flue gas, with exception of steam, is calculated via the ideal gas law:

$$\dot{N}_{i,\mathrm{out}} = Q^*_{\mathrm{T,dry}} y_{i,\mathrm{out,dry}} \frac{\rho_{i,\mathrm{STD}}}{MW_i} \tag{2}$$

With $i = \mathrm{CO_2}$, CO, $\mathrm{CH_4}$, $\mathrm{H_2}$, and $\mathrm{N_2}$. The molar flowrate of steam in the fuel reactor flue gas is calculated assuming a closed hydrogen balance:

$$\dot{N}_{\mathrm{H_2O,out}} = 2\dot{N}_{\mathrm{CH_4,in}} - 2\dot{N}_{\mathrm{CH_4,out}} - \dot{N}_{\mathrm{H_2,out}} \tag{3}$$

The resulting mole fractions on a wet basis in the fuel reactor flue gas can then be calculated:

$$y_{i,\mathrm{out}} = \frac{\dot{N}_{i,\mathrm{out}}}{\dot{N}_{\mathrm{T,out}}} \tag{4}$$

With $\dot{N}_{\mathrm{T,out}} = \Sigma\dot{N}_{i,\mathrm{out}}$ for $i = \mathrm{CO_2}$, CO, $\mathrm{CH_4}$, $\mathrm{H_2}$, and $\mathrm{N_2}$. The resulting volumetric flowrate of the flue gas exiting the fuel reactor is then

$$Q_{\mathrm{T}} = \frac{Q_{\mathrm{T,dry}}}{1 - y_{\mathrm{H_2O,out}}} \tag{5}$$

The resulting performance parameters are calculated based on the preceding equations for calculating molar and volumetric flowrates, as summarized in Table 1. This list consists of methane conversion (both in general and to $\mathrm{CO_2}$ directly), carbon balance, oxygen carrier conversion (based on the estimated solids circulation rate), and average gas residence time.

Table 1. Performance parameters measured in the system.

Parameter	Equation	Parameter	Equation
Carbon balance	$C_{\mathrm{bal}} = \frac{\dot{N}_{\mathrm{CH_4,out}} + \dot{N}_{\mathrm{CO_2,out}} + \dot{N}_{\mathrm{CO,out}}}{\dot{N}_{\mathrm{CH_4,in}}}$	Oxygen carrier conversion	$X_{OC} = \frac{\dot{N}_{O,out}}{\dot{N}_{O,total}}$
Methane conversion	$X_{\mathrm{CH_4}} = \frac{\dot{N}_{\mathrm{CH_4,in}} - \dot{N}_{\mathrm{CH_4,out}}}{\dot{N}_{\mathrm{CH_4,in}}}$		$\dot{N}_{O,total} = \dot{m}_{OC}\left(\frac{3f_{Fe_2O_3}}{MW_{Fe_2O_3}} + \frac{f_{CuO}}{MW_{CuO}}\right)$ $\dot{N}_{O,out} = \dot{N}_{H_2O,out} + 2\dot{N}_{CO_2,out} + \dot{N}_{CO,out}$
Methane conversion to $\mathrm{CO_2}$	$X_{\mathrm{CH_4 \rightarrow CO_2}} = \frac{\dot{N}_{\mathrm{CO_2,out}}}{\dot{N}_{\mathrm{CH_4,in}}}$	Gas residence time	$\tau_{g,FR} = \frac{h_{bed,FR}}{U_{g,LM}}$ $U_{g,LM} = \frac{1}{A_{FR}} \frac{Q_{T,wet} - Q_{in}}{ln\left(\frac{Q_{T,wet}}{Q_{in}}\right)}$

There have been various carriers tested in the NETL CLR. The two oxygen carriers reported in this paper are 1) a raw hematite ore, and 2) a synthetic copper-oxide/iron-oxide hybrid material. The hematite ore was procured from Cliffs Natural Resources Wabush mine in Newfoundland, Canada. The ore was not modified, except for drying and screening to the desired particle size range. The synthetic carrier was developed at NETL and consists of iron oxide and copper oxide supported on alumina, as reported by Siriwardane et al. (2013). Properties of the oxygen carriers reported in this work are shown in Table 2. The particle size and sphericity were determined using the Sympatec QICPIC image analysis system. The minimum fluidization was estimated using a small fluidized bed at room temperature, while the terminal velocities were calculated using correlations from Kunii and Levenspiel (1991). Chemical composition of the carriers was determined using X-ray fluorescence.

Each reactor operated in a slightly different flow regime, as plotted in Fig. 3. The plot shows the dimensionless particle size plotted against the dimensionless gas velocity for the fuel reactor, the air reactor, and the riser

section for both the raw hematite carrier and the synthetic copper-iron carrier. Both carriers act as Geldart group B particles. Even though the hematite is denser, the mean particle size is smaller, so its effective particle size is still smaller. The fuel reactor is operated slightly below that for conventional fluidized beds to minimize entrainment of solids into the freeboard. Meanwhile, the air reactor is operated in the turbulent regime near the terminal velocity of the particles. The riser is operated in the circulating fluidized bed regime.

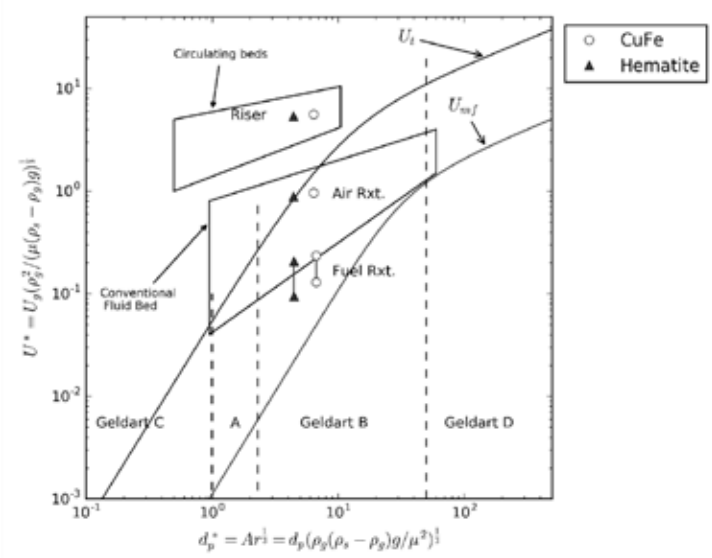

Fig. 3. Flow regime map showing where the air reactor, fuel reactor, and riser operate in the CLR. Map based on plot from Grace (1986).

Table 2. Properties of the oxygen carriers reported in this work.

Property	Hematite	CuFe	Units	Source
Hydrodynamic Characteristics				
Sauter Mean Diameter (d_{32})	210	343	µm	Sympatec QICPIC
Sphericity	0.876	0.91	--	“”
Particle density	4900	2900	kg/m^3	
Bulk density	2940	1430	kg/m^3	Measured
Minimum Fluidization Velocity	0.09	0.14	m/s	Measured
Terminal Velocity (25°C)	1.99	2.36	m/s	Formula from Kunii and Levenspiel (1992)
Terminal Velocity (900°C)	1.747	2.52	m/s	“”
Chemical Characteristics				
Fe_2O_3	86.6	31	wt%	XRF analysis
CuO	--	37	wt%	“”
Al_2O_3	--	31	wt%	“”
MnO	3.4	--	wt%	“”
SiO_2	10	--	wt%	“”

RESULTS AND DISCUSSION

Table 3 shows a summary of key results from both runs. Tables of complete results can be found in Weber et al. (2016) for the raw hematite, and Bayham et al. (2016) for the synthetic carrier. Representative results are shown here for broader comparison. The first two columns consist of the lowest and highest conversion results from the raw hematite oxygen carrier, and the last four columns are results for the synthetic copper-iron oxygen carrier. For the copper-iron carrier, two sets of results are presented: results for a long-term test of around ten hours, and results from an attempt at “autothermal” conditions, whereby the electric gas preheaters were shut off to force the only source of energy to come from the chemical looping reactions. While the system could run without natural gas addition to the air reactor and with no electric preheat, residual heat was still present in the refractory.

The reactor temperatures were higher for the raw hematite, and the methane conversion was lower than the copper-iron material. Subsequently, the supplemental natural gas added to the air reactor to overcome heat losses was also higher for the hematite. In general, the overall methane conversion was higher than the specific methane conversion to carbon dioxide for both materials. This is most likely due to production of carbon monoxide and possible carbon deposition.

From aeration-gas cutoff tests (Weber et al. 2016, Bayham et al. 2016), it was noted that the estimated solids circulation rate for the copper-iron material was lower than the hematite. Since the flow rate of solids through the L-valve is a function of the weight of solids in the standpipe, the circulation rate on a mass basis was on average around three times higher and on a volumetric basis and almost two times higher with the higher density hematite carrier. The oxygen carrier utilization for the copper-iron material was higher and these results suggest that the synthetic copper-iron material can operate at a lower circulation rate, higher fuel conversion, and lower temperature than the hematite ore.

Table 3. Results for copper-iron oxygen carrier.

	Raw Hematite		CuFe Long Trials		CuFe "Autothermal"	
	Lowest Conv.	Highest Conv.	1A	1B	2A	2B
Trial time (min)	51	56	301	284	29	29
Fuel Reactor Temperature (°C)	882	945	818	844	822	814
Air Reactor Temperature (°C)	946	1006	878	899	956	953
Fuel Reactor Pressure (kPa)	157	157	159	160	161	161
Inventory (kg)	55	56	50	48	34	34
Gas Residence Time FR (s)	1.00	1.88	2.24	1.80	1.13	1.12
Solids Residence Time FR (s)	235	243	720	1901	294	313
Fuel Reactor Bed Height (m)	0.436	0.458	0.61	0.57	0.32	0.32
Air Reactor Bed Height (m)	0.346	0.331	0.52	0.52	0.48	0.47
Molar Flow CH_4 FR in (mol/h)	121	60	40	86	185	191
Molar Flow N_2 FR in (mol/h)	708	359	498	493	283	282
Molar Flow CH_4 AR in (mol/h)	113	115	88	49	0	0
Carbon Balance (%)	103.2%	98.5%	99.8%	97.7%	93.8%	94.3%
Methane Conversion to CO2 (%)	9.2%	35.2%	65.4%	64.7%	65.3%	63.6%
Methane Conversion (%)	7.3%	40.9%	66.1%	67.6%	72.5%	70.5%
Circulation Rate (kg/h)	508	519	153	125	194	182
Oxygen Carrier Utilization (%)	0.5%	1.2%	6.8%	37.8%	25.4%	27.2%

Further comparison can be made through plotting the performance results of both carriers on the same plot. Fig. 4 shows the effect of temperature on the overall methane conversion and the methane conversion to carbon dioxide, for both oxygen carriers. The performance results consist of all the test trials. As shown, both carriers show distinct improvement in conversion as the fuel reactor temperature increases. Furthermore, the methane conversion with the copper-iron material is generally higher than the hematite, despite the lower reactor temperatures and lower circulation rates.

Fig. 5 shows the flowrate of each species in the fuel reactor flue gas, namely hydrogen, carbon monoxide, and natural gas, as a function of the potential natural gas thermal input, or fuel flow, into the fuel reactor. The unconverted product gases are higher for the hematite than the copper-iron. However, there seems to be a point above 30 kW_{th} where the bed cannot convert the methane products to CO_2 for the copper-iron material and the hydrogen, carbon monoxide, and methane flowrates increase dramatically. In a potential chemical looping plant, the flue gas exiting the fuel reactor should consist of only carbon dioxide and steam. The combined mole concentration of carbon dioxide and steam without the diluent nitrogen is shown in Fig. 6. As shown, the combined steam and carbon dioxide mole concentration is around 80% for the copper-iron oxygen carrier for a wide range of natural gas input flows, while the hematite test data is strongly dependent on the fuel feed rate. This can also be seen in the methane conversion, which is also plotted in Fig. 6. The independence of the methane conversion and the natural gas feed input is indicative of mass-transfer limitations between the bubble and the emulsion, cloud, or wake solids. This observation is consistent with previous results (Siriwardane et al. 2013) that indicate these synthetic carriers are more porous and reactive compared to raw ores.

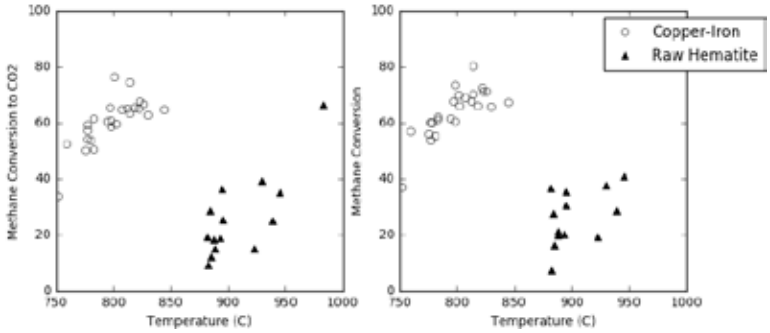

Fig. 4. Effect of temperature on the conversion of natural gas in the fuel reactor.

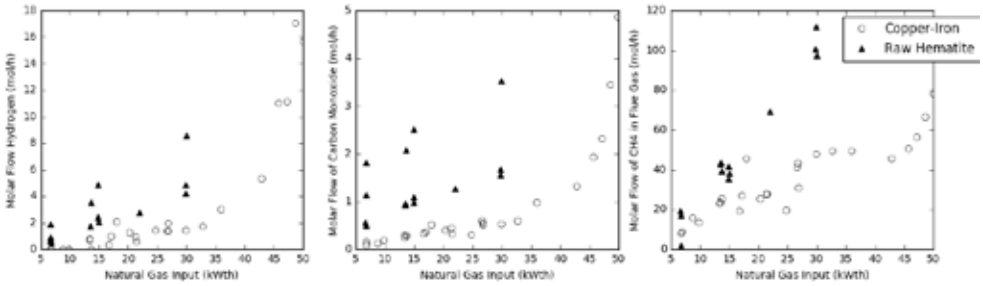

Fig. 5. Molar flow rates of product gases for each trial for the raw hematite and synthetic carrier.

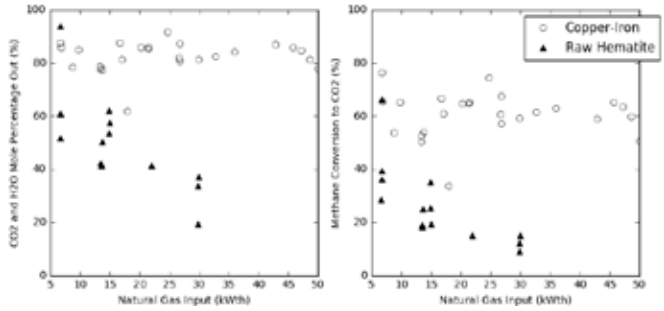

Fig. 6. (a) Species purities for CO_2 and steam (minus the nitrogen diluent) and (b) Methane conversion to CO_2 as a function of natural gas input.

CONCLUSIONS

The performance of two representative oxygen carriers tested in the U.S. Department of Energy NETL's chemical looping reactor test rig has been reported, namely, a raw hematite ore, which is considered cheap, and a synthetic copper-iron material. Hematite is a relatively inexpensive material, but poor fuel conversion was observed during this testing. The synthetic copper-iron-alumina material demonstrated better fuel conversion, despite operating at lower reactor temperatures and lower carrier circulation rates. However, manufacturing costs for synthetic oxygen carriers like the copper-iron-alumina material are a significant concern.

Due to the high endothermicity of the raw hematite carrier reduction reaction, the system was operated at a higher temperature than the copper-iron material, ranging between 880-944°C. The resulting methane conversion ranged between 9-35%, depending on the gas residence times, temperature, and natural gas feed fractions.

The operation of the manufactured copper-iron-alumina carrier required a lower operating temperature than the hematite because of the presence of copper, namely between 751-844°C. For the testing of the copper-iron material, the natural gas input to the fuel reactor ranged between 6.7 and 50.0 kW_{th} and a fuel reactor natural gas feed concentration between 5 - 42 vol.%. Due to the neutral heat of reaction in the fuel reactor for the copper-iron material, the operations could be performed without natural gas combustion in the air reactor to supplement the heat. The gas residence times ranged from 0.5 - 1.5 seconds, and the oxygen carrier residence times ranged from around 3 to 15 minutes. Calculated from the gas analysis and the inlet flows during the trials, the methane conversion to CO_2 ranged from 33.9% to 76.5%, which is significantly higher than the hematite even at lower fuel reactor temperatures. Additionally, the solids circulation rate for the manufactured copper-iron carrier was estimated to be lower than that for the raw hematite carrier for the same aeration gas settings.

Although further study is required, the copper-iron-alumina oxygen carrier material demonstrated performance that was consistent with mass-transfer limitations, whereas the hematite oxygen carrier did not seem to be limited by the mass transfer between the bubble, cloud, and emulsion in the fluidized bed. Future work is planned to investigate the copper-iron-alumina oxygen carrier material at higher fuel inputs.

ACKNOWLEDGMENTS

The authors would like to acknowledge the financial and technical support of DOE's Advanced Combustion Program. The authors would also like to acknowledge the dedication and diligence of the operating and support staff that include: Dave Reese, Jeffrey Riley, Mark Tucker, Richard Eddy, Stephen Carpenter, and the late James Spenik. Dr. Ranjani Siriwardane, Jarrett Riley, William Benincosa, and Dr. Hanjing Tian have also played a critical role in this effort as the research team that developed the synthetic oxygen carrier material reported in this work. Without the contributions of these people, this work would not be possible. The authors would also like to thank the developers of Python, Pandas, Numpy, Scipy, Matplotlib, Seaborn, and Jupyter for the fantastic data analysis tools.

DISCLAIMER

NOTATION

A_{FR}	Cross sectional area of fuel reactor (m^2)
C_{bal}	Carbon balance term (ratio of carbon atoms out divided by carbon atoms in) (-)
d_p	Particle size (m)
f_i	Weight fraction of species in oxygen carrier (i = Fe_2O_3, CuO) (kg/kg)
$h_{\text{bed,FR}}$	Height of solids in fuel reactor (m)
$\dot{m}_{\text{OC}}$	Solids circulation rate (kg/h)
MW_i	Molecular weight of species i (kg/mol)
$\dot{N}_{\text{T,out}}$	Total molar flow rate of the flue gas (mol/h)
$\dot{N}_{i,\text{in}}$	Molar flowrate of species i into the reactor (mol/h)
$\dot{N}_{i,\text{out}}$	Molar flowrate of species i in the flue gas (mol/h)
$\dot{N}_{\text{O,out}}$	Molar flowrate of atomic oxygen out of the fuel reactor (mol/h)
$\dot{N}_{\text{O,total}}$	Total molar oxygen flow rate contained in the solid (mol/h)
$Q^*_{\text{N}_2,\text{in}}$	Total standard nitrogen volumetric flow rate (SCFH)
Q_{LM}	Log-mean average volumetric flow rate (SCFH)
$Q^*_{\text{T,dry}}$	Total dry volumetric flow rate (SCFH)
$Q^*_{\text{T,wet}}$	Total standard volumetric flow rate on a wet basis (SCFH)
$Q_{\text{T,wet}}$	Total volumetric flow rate on a wet basis (SCFH)
Q_{in}	Volumetric flow rate in (SCFH)
U_g	Gas velocity (m/s)

$U_{\mathrm{g,LM}}$	Log-mean averaged gas velocity (m/s)
$X_{\mathrm{CH_4}}$	Methane conversion (%)
$X_{\mathrm{CH_4 \rightarrow CO_2}}$	Methane conversion to carbon dioxide (%)
X_{OC}	Oxygen carrier conversion or utilization (mol/mol, %)
$y_{i,\mathrm{out,dry}}$	Mole fraction of species *i* in flue gas on a dry basis
$y_{i,\mathrm{out}}$	Mole fraction of species *i* in the flue gas on a wet basis
μ	Gas viscosity (Pa-s)
ρ_g	Gas density (kg/m^3)
ρ_p	Particle density (kg/m^3)
$\rho_{i,\mathrm{STD}}$	Density of gaseous species *i* at standard temperature and pressure (kg/m^3)
$\tau_{\mathrm{g},i}$	Gas residence time in reactor *i* (s)

REFERENCES

Adanez, J.; Abad, A.; Garcia-Labiano, F.; Gayan, P.; de Diego, L. 2012. Progress in Chemical-Looping Combustion and Reforming Technologies. Progress in Energy and Combustion Science, 38, 215-282.

Adanez, J.; Gayan, P.; Celaya, J.; de Diego, LF.; García-Labiano, F.; Abad, A. 2006. Chemical Looping Combustion in a 10 kW Prototype Using a CuO/Al_2O_3 Oxygen Carrier: Effect of Operating Conditions on Methane Combustion. Industrial and Engineering Chemistry Research, 45, 6075-6080.

Bayham, S.; Straub, D.; Weber, J., 2016. Operation of the NETL Chemical Looping Reactor with Natural Gas and a Novel Copper-Iron Material. NETL-PUB-20912; NETL Technical Report Seriews; U.S. Department of Energy, National Energy Technology Laboratory: Morgantown, WV. In Press.

Ciferno, J.; Litynski, J.; Brickett, L.; Murphy, J.; Munson, R.; Zaremsky, C.; Marano, J.; and Strock, J. 2011. DOE/NETL Advanced CO2 Capture R&D Program: Technology Update. U.S. Department of Energy, Morgantown, WV.

Grace, J.R. 1986. Contacting Modes and Behaviour Classification of Gas-Solid and Other Two-Phase Suspensions. Canadian Journal of Chemical Engineering 64, 353-363.

Kunii, D.; Levenspiel, O. 1992. Fluidization Engineering. Butterworth-Heinemann, Newton, MA.

Linderholm, C.; Schmitz, M.; Knutsson, P.; Lyngfelt, A. 2016. Chemical-Looping Combustion in a 100-kW Unit Using a Mixture of Ilmenite and Manganese Ore as Oxygen Carrier. Fuel, 166, 533-542.

Shen, L.; Wu, J.; Xiao, J.; Song, Q.; Xiao, R. 2009. Chemical-Looping Combustion of Biomass in a 10 kW Reactor with Iron Oxide as an Oxygen Carrier. Energy and Fuels, 23. 2498-2505.

Siriwardane, R.; Tian, H.; Simonyi, T.; Poston, J. 2013. Synergetic Effects of Mixed Copper-Iron Oxides Oxygen Carriers in Chemical Looping Combustion. Fuel 108, 319-333.

Weber, J.; Straub, D.; Breault, R.; Richards, G., 2014. Operating Experience of a Chemical Looping Circulation Fluidized Bed Combustor. Proceedings of the International Clearwater Coal Conference, Clearwater, FL, USA.

Weber, J.; Straub, D.; Bayham, S.; Breault, R.W., 2016. Operating Experience of a 50kWth Methane Chemical Looping Reactor. Proceedings of Fluidization XV, Montebello Quebec, Canada.